*The Canadian Mineralogist*
Vol. 50, pp. 815-824 (2012)
DOI : 10.3749/canmin.50.4.815

# ALLANITE-(Nd) FROM THE KINGMAN FELDSPAR MINE, MOJAVE PEGMATITE DISTRICT, NORTHWESTERN ARIZONA, USA

Sarah L. HANSON[§]

*Geology Department, Adrian College, 110 S. Madison Street, Adrian, Michigan 49221, USA*

Alexander U. FALSTER, William B. SIMMONS and TJ A. BROWN

*Department of Earth and Environmental Sciences, University of New Orleans, 2000 Lakeshore Drive,*
*New Orleans, Louisiana 70148, USA*

## Abstract

The Kingman pegmatite, located in the Cerbat Range in northwestern Arizona, is hosted by orogenic 1.7 Ga Paleoproterozoic granitic rocks. This post-orogenic pegmatite was intruded into these granites during the middle Proterozoic (*ca*. 1.5 Ga) subsequent to the Yavapai and Mazatzal orogenies. Extreme LREE-enrichment, as well as the HREE-depletion, is exemplified by the presence of abundant large crystals of LREE-enriched allanite and a near-absence of HREE-enriched minerals. Most of the allanite is Nd-rich allanite-(Ce). However, several of the samples have domains that are Nd-dominant, and thus are allanite-(Nd). This represents the fourth world location and the first reported U.S. location for allanite-(Nd). The Nd-dominant domains, which typically occur near the rim of grains and along fractures, may be the result of alteration by highly oxidizing late-stage fluids that replaced allanite with bastnäsite-(Ce). Late-stage carbonate fluids, enriched in F from the dissolution of biotite, could have preferentially redistributed Ce into bastnäsite-(Ce), resulting in Nd-enriched recrystallized allanite near fractures and along the recrystallized rim. As the Kingman pegmatite is not associated with a parental granite and as it exhibits unusual depletions in F, Nb, Ta, and HREE and an extreme enrichment in the LREE, we favor an anatectic origin.

*Keywords*: allanite-(Nd), allanite-(Ce), Kingman granitic pegmatite, Mojave pegmatite district, Arizona.

## Introduction

The Kingman granitic pegmatite is one of five large bodies recently studied in the Mojave pegmatite district in northwestern Arizona. The Mojave pegmatites were uplifted and exposed as a result of block faulting during Basin and Range extension in the Tertiary. The Kingman pegmatite crops out near the southeastern base of the Cerbat Range approximately a kilometer and a half northwest of Kingman, Arizona. The other four bodies of pegmatite lie approximately 65 km southeast of Kingman on the western flank of the Aquarius Range. The Kingman pegmatite is unique in the Mojave District as it is the only body that is intrusive into older host granite and not associated with a genetically related host pluton. The Kingman pegmatite is enriched in the rare-earth elements (REE), yet minerals composed of the heavy rare-earth elements (HREE), F, Nb are conspicuously absent. Instead, the pegmatite exhibits an extreme enrichment in light rare-earth elements (LREE) as allanite is the only REE mineral present; it occurs as abundant and large crystals. Some allanite crystals exhibit variable dominance in REE as they have Ce-dominant cores with domains along the rims and fractures that are Nd-dominant. The purpose of this study is to characterize the unusual REE profiles exhibited by both the pegmatite and the allanite crystals.

## General Geology

The Mojave district pegmatites lie within the eastern portion of the Mojave province, a terrane that underlies much of present-day extreme northwestern Arizona, southeastern California, southern Nevada and southwestern Utah. The Mojave province is composed predominantly of recycled crustal material that, on the basis of zircon chronology from metasedimentary rocks, is as old as 2.830 Ga (Wooden & Miller

---

[§] *E-mail address*: slhanson@adrian.edu

1990, Wooden *et al.* 1988, Duebendorfer *et al.* 2001). Juxtaposition of the Mojave terrane with the adjacent juvenile Yavapai terrane occurred between 1.740 and 1.720 Ga (Duebendorfer *et al.* 2001). The sutured Mojave and Yavapai terranes docked with Laurentia during the Yavapai Orogeny (1.710–1.680 Ga) as part of a progressive amalgamation that added new crust to southern Laurentia (Whitmeyer & Karlstrom 2007, Duebendorfer *et al.* 2001).

Plutons in the Cerbat Mountains are orogenic and range in age from 1.768 ± 5.5 Ga to 1.719 ± 1.2 Ga, thus are generally contemporaneous with the justaposition of the Mojave and Yavapai terranes (Duebendorfer *et al.* 2001). Large exposures of the youngest of these plutons, the Diana granite, crop out in the western and eastern Cerbat Range (Duebendorfer *et al.* 2001). On the basis of textural similarities, it is inferred to be the granitic massif into which the Kingman pegmatite is intruded. These plutonic rocks are a medium grained, porphyritic granodiorite to quartz diorite with microcline megacrysts up to 1.2 cm across.

Like all bodies of pegmatite in the Mojave pegmatite district, the Kingman pegmatite has a distinctive anorogenic chemical signature, which includes LREE enrichment. Microcline from the Kingman pegmatite yielded a $^{87}$Sr–$^{87}$Rb age of *ca.* 1.550 Ga (Wasserburg & Lanphere 1965), whereas electron-microprobe-derived ages on monazite from a satellite quarry yielded an average age of 1.561 ± 37 Ga. Thus, these pegmatites are related to post-orogenic extensional magmatism that occurred subsequent to the Yavapai and Mazatzal orogenies between approximately 1.3 and 1.6 Ga, generally referred to as *ca.* 1.4 Ga magmatism. The nature of this extension remains controversial and has been attributed to back-arc extension in a broadly compressional regime (McLelland *et al.* 1996, 2010, Kay & Mahlburg-Kay 1993, Condie 1986) as well as to a broadly extensional regime following a supercontinent breakup (Windley 1993). Regardless of whether the tectonic regime was broadly compressional with localized extension or broadly extensional, the Mojave pegmatites are distinctly anorogenic in character and record an extensional event in northwestern Arizona (Simmons *et al.* 2011).

## THE KINGMAN PEGMATITE

The Kingman pegmatite is a sill-like body that trends N50–65°E, dips 60–75°NW and ranges in thickness from 20 to 60 m, with a general widening to the northeast (Heinrich 1960). The pegmatite is exposed over approximately 500 meters. Approximately 1.5 km to the southwest of the main quarry, roughly along strike with the Kingman pegmatite, a small prospect pit exposes a small portion of the northern edge of a larger body of pegmatite that may be a continuation of the Kingman pegmatite.

Contacts between the pegmatite and the older host granitic rocks into which they were intruded are well defined and, in some locations, exhibit reaction boundaries 0.3 m wide with the host granite. A distinct ~0.5 m border zone composed of white, aplitic quartz and feldspar is present along the contact. Feldspar mining in the 1950s opened three main cuts into the pegmatite, which herein will be referred to as A, B and C. In cuts B and C (Fig. 1), much of the pegmatite has been removed, in some areas down to the country rock. Where wall-zone material is exposed, abundant allanite is present. Approximately 150 m to the northeast of Cut B is a third pit, Cut A, that exposes both wall zone and core of the pegmatite as well as the host pluton. Along the northwest wall of the cut, a nearly horizontal diabase dike (0.1–0.6 m) cuts the pegmatite. There are also several roof pendants of gneissic metamorphic rocks exposed within the granite and pegmatite. Allanite is notably absent from Cut A.

The Kingman pegmatite is zoned, with a thin discontinuous border zone that ranges from 0.1 to 0.5 m thick and is composed almost entirely of microcline and fine-grained quartz. The wall zone ranges in thickness from 3 to 6 m, with an average of approximately 4 m. It is comprised predominantly of quartz and white microcline with lesser biotite and accessory allanite, magnetite, zircon, titanite, bastnäsite, uraninite, apatite, hematite, ilmenite and rutile. In Cut A only, small amounts of muscovite and rare millimeter-sized crystals of garnet also are present. The composite quartz–microcline core ranges in thickness from 10 to 60 m, with microcline masses averaging 3–4 m across and less abundant pods of grey quartz that reach approximately 2 × 2 × 5 m (Heinrich 1960). Locally, stringers of quartz from the quartz pods cut through the large microcline masses.

The Kingman Feldspar pegmatite exhibits an unusual REE mineral assemblage; HREE-bearing minerals are conspicuously absent. Only one small (~1 cm) mass of aeschynite-(Y) was recovered from material slumped off the east wall in the satellite quarry (Hanson *et al.* 2007). Conversely, the only LREE phase, allanite, is abundant in the Kingman mine; it occurs as unusually large and abundant crystals. Heinrich (1960) reported that during one excavation in 1944, approximately 20 tonnes of allanite were sent to an unknown buyer. Within the small satellite prospect pit, two large pods (up to 30 cm) of monazite-(Ce) are exposed on the western wall of the cut (Hanson *et al.* 2007). Fluorite is notably absent. Thus the pegmatites are strongly enriched in LREE and extremely depleted in Nb, HREE, and F. These chemical characteristics are atypical for classic niobium–yttrium–fluorine (NYF) pegmatites as described by Černý & Ercit (2005).

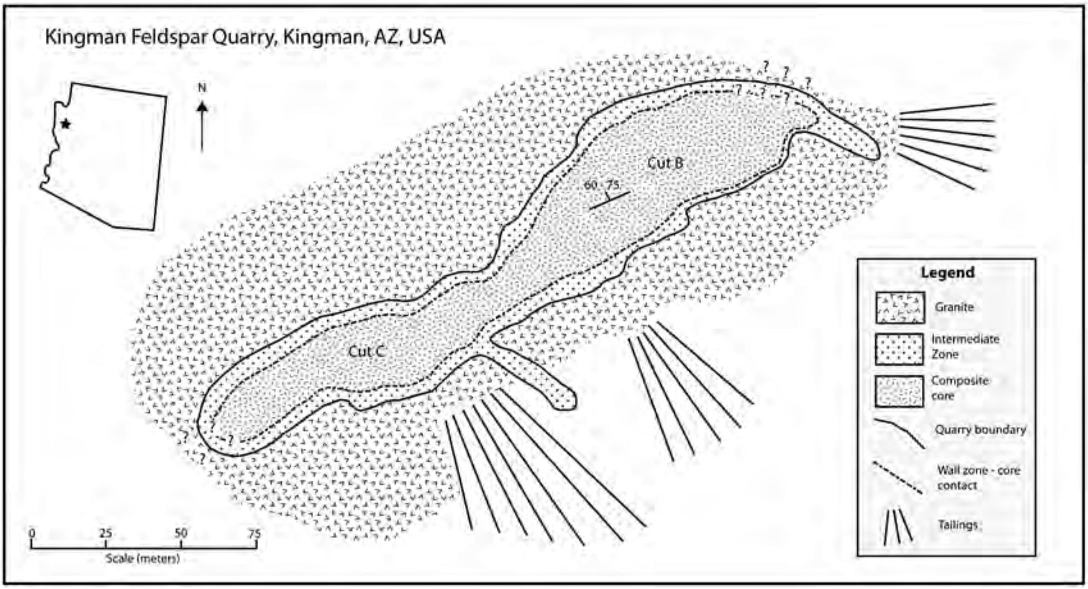

FIG. 1. Sketch map of cuts B and C at the Kingman Feldspar mine. The boundary of the quarry generally corresponds to the pegmatite – granite contact except at the northeastern and southwestern edges of the quarry, where it is not exposed.

## ALLANITE

Until recently, there were only three recognized species making up the allanite subgroup, ideally [CaREE,Y,$Fe^{2+}Al_2(Si_2O_7)(SiO_4)O(OH)$]. These include allanite-(Ce), allanite-(La) and allanite-(Y). A new species, allanite-(Nd), discovered in an NYF pegmatite near Åskagen, Värmland, Sweden, was recently approved by the IMA (Škoda *et al.* 2010). In addition, two previous reports of Nd-dominant allanite predate IMA approval. These include specimens from granitic pegmatites near Madrid (Gonzalez del Tánago 1997) and Japan (Minakawa *et al.* 2001).

In the Kingman pegmatite, allanite occurs as large, extensively fractured pods or crude crystals up to nearly a half meter in size on the south wall of cuts B and C. The individual crystals are nearly to completely metamict, dark brown to black in color, euhedral to subhedral, and reach ~25 cm in length. All of the exposed surfaces of allanite are coated with a reddish iron oxide crust and locally with Nd-enriched bastnäsite-(Ce). Microscopic inclusions of thorogummite occur within the allanite.

## ANALYTICAL METHODS

X-ray-diffraction analyses were carried out at the University of New Orleans using a Scintag XDS–2000 X-ray diffractometer at a scan rate of 2° 2θ per minute. Standards for calibration include corundum and quartz. Cell parameters were calculated using reflections between 8 and 57° 2θ with CELL, a modified IBM–PC version of the least-squares refinement program of Appleman & Evans (1973).

The chemical composition of the allanite was measured at the University of New Orleans on an ARL–SEMQ electron microprobe with an acceleration voltage of 15 kV and a beam current of 15–20 nA. Peak counts were collected for 45 seconds, and background positions were determined by the mean atomic number (MAN) method. Standards are as follows with detection limits in parentheses: synthetic REE orthophosphates ($L\alpha$ for La, Ce, Eu, Gd, Tb, Ho, Tm, Yb, Lu and $L\beta$ for Pr, Nd, Sm, Dy and Er) (0.010), synthetic $YPO_4$ (Y) (0.010), synthetic PbO (Pb) (0.012), synthetic $UO_2$ (U) (0.010), synthetic $ThO_2$ (Th) (0.010), albite (Na) (0.014), orthoclase (K) (0.011), diopside (Mg) (0.012), Ca (0.008) and Si), fayalite (Fe) (0.008), rutile (Ti) (0.008), spessartine (Mn) (0.009), and topaz (F) (0.015). Matrix effects were corrected using a $\phi(\rho Z)$ correction procedure (Pouchou & Pichoir 1991).

## X-RAY DIFFRACTOMETRY

Owing to the metamict nature of the allanite, heating was required prior to X-ray-diffraction analysis. Metamict samples were heated to 700°C for 12 hours in a slightly reducing atmosphere, achieved using a mixture of 95% Ar and 5% $H_2$ as described by Sugitani *et al.* (1984, 1985) (Fig. 2). An indexed pattern of heated allanite (JCPDS #9–474) is compared to peaks for allanite-(Nd) in Table 1. Cell parameters are given in Table 2. The similarity of this pattern to the JCPDS heated allanite as well as the similarity of the cell edges confirm the allanite structure of this mineral.

## CHEMICAL COMPOSITION

The bulk composition and chemical formulae for selected allanite samples from Kingman are given in Table 3. Oxide totals were initially recalculated on the basis of eight cations. Subsequently, $Fe^{2+}$ and $Fe^{3+}$ were partitioned to yield a total of 25 positive charges. The amount of $H_2O$ was calculated by stoichiometry to yield a total of (OH + F + Cl = 1 *apfu*). Site occupancies were allotted according to the method suggested by Armbruster *et al.* (2006). The species affiliation for each sample was determined using both *A*2 and *M*3 site occupancies in a method proposed by Ercit (2002). Ercit (2002) showed that a series *A*2 and *M*3 substitutions may produce epidote–clinozoisite *versus* allanite-(La), and allanite-(La) and allanite-(Y) *versus* a hypothetical end-member devoid of Fe. He further suggested that the relative proportions of these end members are best differentiated using combined expressions that are based on cation occupancies of the *A*2 and *M*3 sites. A plot of these expressions (Fig. 3) shows that all samples have sufficient REE (Ln) and divalent *M*3 cations to place them in the allanite group rather than the epidote group of minerals.

TABLE 1. X-RAY POWDER-DIFFRACTION PATTERN OF ALLANITE-(Nd)

| JCPDS #9-474 allanite, heated | | | Allanite-(Nd) heated to 700°C | | | |
|---|---|---|---|---|---|---|
| *I* | *d* | *hkl* | *I* | *d* (obs) | *d* (calc) | *hkl* |
| 30 | 9.30 | 100 | 20 | 9.222 | 9.157 | 100 |
| 30 | 5.07 | 101, 201 | 25 | 5.059 | 5.063 | $\bar{1}01$ |
| 10 | 4.84 | 110 | | | | |
| 10 | 4.67 | 011, 111 | | | | |
| 50 | 4.62 | 200 | 15 | 4.646 | 4.643 | $\bar{1}11$, 200 |
| 3 | 4.43 | $\bar{1}02$ | | | | |
| 3 | 4.10 | 002 | | | | |
| 20 | 4.00 | $20\bar{2}$ | 20 | 4.010 | 4.001 | $\bar{2}02$ |
| 10 | 3.81 | $\bar{2}11$, 111 | 6 | 3.784 | 3.782 | 111 |
| 1 | 3.60 | 210 | | | | |
| 80 | 3.50 | $\bar{1}12$ | 60 | 3.509 | 3.504 | $\bar{1}12$ |
| 30 | 3.34 | 012 | | | | |
| 20 | 3.27 | $\bar{2}12$ | 10 | 3.280 | 3.270 | $\bar{2}12$ |
| 10 | 3.20 | 102, $\bar{3}02$ | 20 | 3.203 | 3.206 | $\bar{3}02$ |
| 100 | 2.96 | $\bar{1}03$, 211 | 100 | 2.925 | 2.919 | $\bar{3}11$ |
| 30 | 2.83 | 020, 112 | 40 | 2.850 | 2.835 | 020 |
| 3 | 2.79 | | 15 | 2.792 | 2.791 | $\bar{3}12$ |
| 30 | 2.74 | | 30 | 2.705 | 2.704 | 310 |
| 80 | 2.67 | | 50 | 2.673 | 2.673 | $\bar{3}03$ |
| 40 | 2.60 | | 40 | 2.606 | 2.612 | $\bar{2}13$ |
| 30 | 2.54 | | 30 | 2.531 | 2.533 | 202 |
| 3 | 2.48 | | | | | |
| 30 | 2.43 | | 20 | 2.420 | 2.421 | $\bar{3}13$ |
| 3 | 2.40 | | 15 | 2.400 | 2.406 | $\bar{1}22$ |
| 10 | 2.33 | | | | | |
| 10 | 2.24 | | | | | |
| 10 | 2.20 | | | | | |
| 30 | 2.16 | | 30 | 2.164 | 2.164 | $\bar{3}04$ |
| 30 | 2.13 | | 20 | 2.129 | 2.125 | 122 |
| 10 | 2.06 | | 20 | 1.926 | 1.927 | $\bar{5}12$ |
| 20 | 1.90 | | 30 | 1.890 | 1.887 | $\bar{4}21$ |
| 30 | 1.65 | | 20 | 1.635 | 1.635 | $\bar{5}21$ |
| 60 | 1.63 | | | | | |

Cu*K*α radiation, λ = 1.54060 Å. Intensities were normalized to the highest peak. Values of *d* are quoted in Å.

Allanite from the Kingman mine is predominantly Nd-rich allanite-(Ce). However, several of the samples from cut B exhibit Nd-dominant domains, and thus are allanite-(Nd) (Fig. 4). In general, the more Nd-enriched areas are located along fractures and near the rim of the crystals. This variability in the dominant cation arises from subtle differences in the relative abundance of Ce and Nd, with Nd/Ce values ranging from 0.57 to 1.51. Thus, the allanite ranges from Ce- to Nd-dominant within distinct domains. Because the chemical differences are small, the individual domains are not readily distinguishable using back-scattered electron microscopy. The Nd-rich domains, however, are generally associated with bastnäsite-(Ce) which occurs as an alteration product along the rim of the allanite grains (Fig. 5). Like allanite-(Nd), the bastnäsite-(Ce) has nearly equal Ce and Nd *apfu* (Fig. 4).

A chondrite-normalized plot of compositions of Kingman allanite shows the significant enrichment in LREE as well as the subtle variations in the Ce and Nd contents (Fig. 6). It is evident from this figure that the allanite-(Nd) is not really Nd-enriched but instead has a relatively slightly lower level of Ce. In addition, both allanite-(Ce) and allanite-(Nd) exhibit unusual spikes in Yb. Ytterbium enrichments in REE minerals are rare, and Yb-dominant REE minerals are generally the result of Y depletion in F-enriched pegmatites, as Y, which is preferentially complexed with F over the other HREE, may remain in the fluid phase (Gramaccioli *et al.* 1999, Gramaccioli & Pezzotta 2000, Simmons *et al.* 2006). The lack of F in the Kingman Pegmatite precludes this mechanism for Yb enrichment. It should be noted, however, that the Yb enrichment may be more apparent than real, as the HREE elements are very low in abundance; the anomaly may simply be the result of analytical error.

TABLE 2. UNIT-CELL PARAMETERS OF ALLANITE-(Nd) HEATED TO 700°C

| | JCPDS #9-474 Allanite heated | Allanite-(Nd) |
|---|---|---|
| *a* (Å) | 10.22 | 10.241(7) |
| *b* (Å) | 5.75 | 5.698(7) |
| *c* (Å) | 8.95 | 8.910(8) |
| β (°) | 115 | 115.75(8) |
| *V* ($Å^3$) | 476.7 | 468.2(6) |

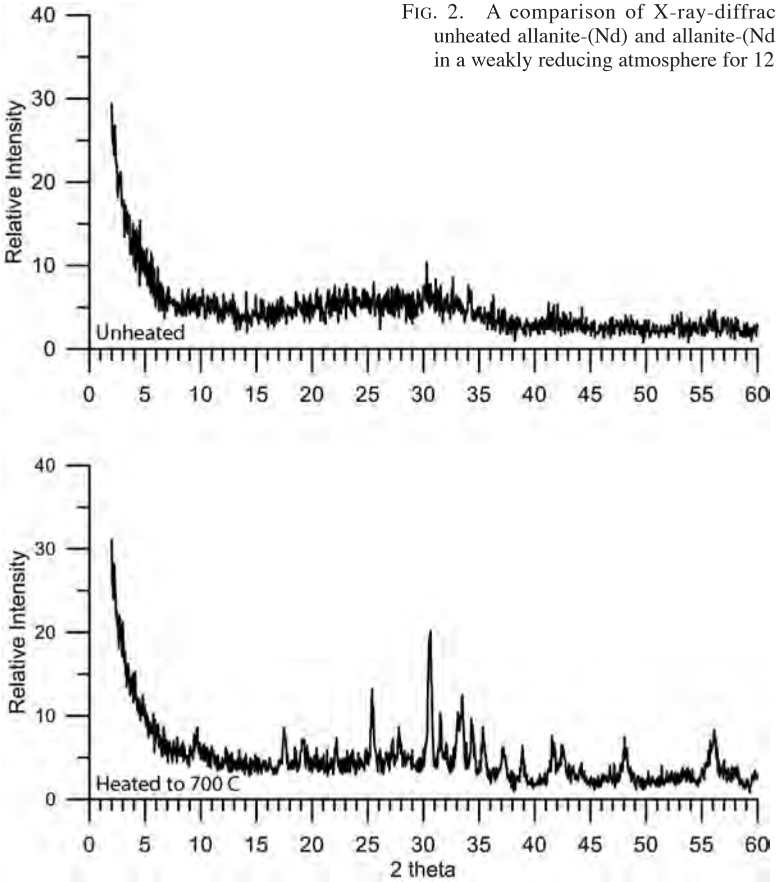

FIG. 2. A comparison of X-ray-diffraction patterns for unheated allanite-(Nd) and allanite-(Nd) heated to 700°C in a weakly reducing atmosphere for 12 hours.

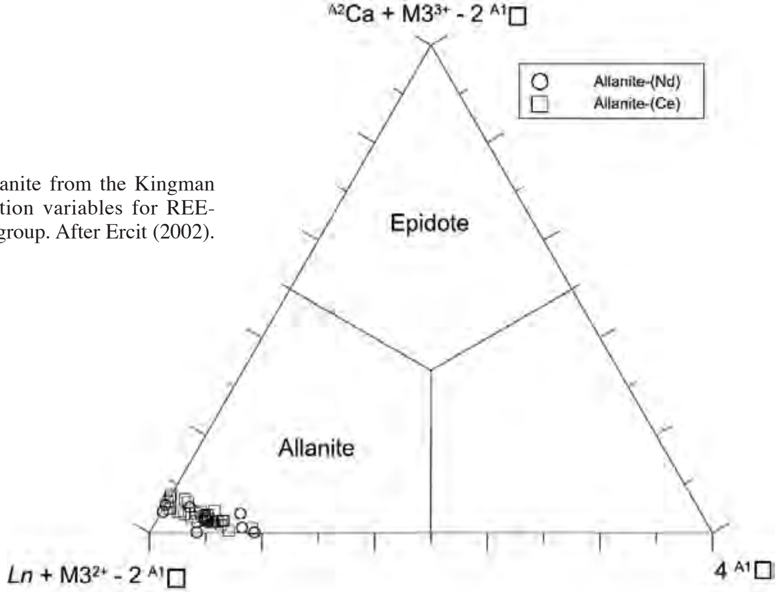

FIG. 3. Chemical variations in allanite from the Kingman pegmatite based on discrimination variables for REE-bearing members of the epidote group. After Ercit (2002).

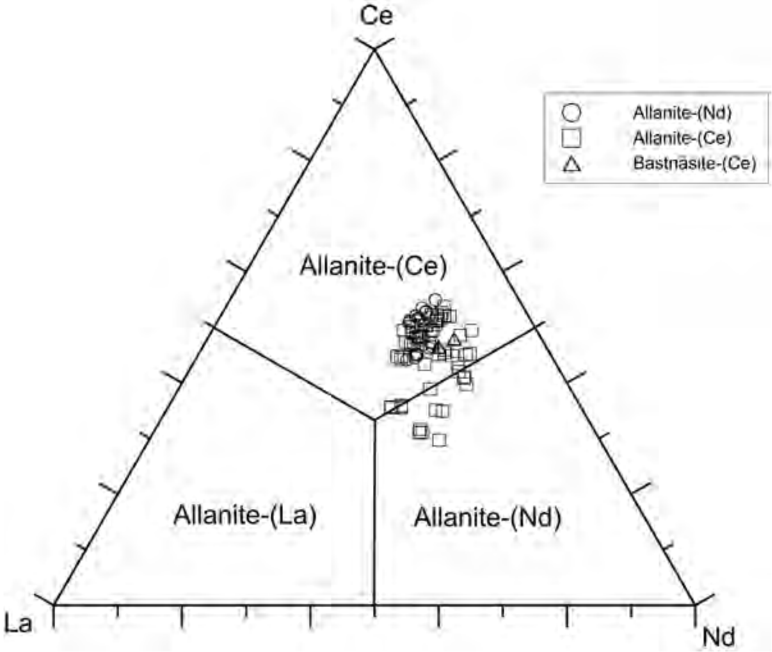

FIG. 4. Distribution of the three dominant REE at the *A*2 site of allanite-(Nd), allanite-(Ce) and bastnäsite-(Ce) from the Kingman pegmatite.

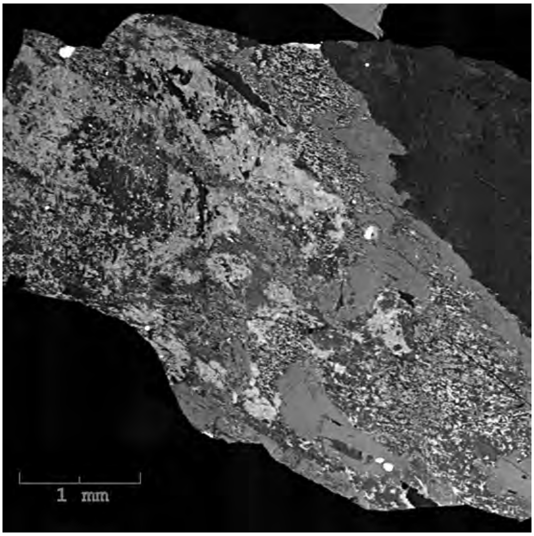

FIG. 5. BSE image showing replacement of allanite with bastnäsite-(Ce). The millimetric medium gray grains in the center of the image consist of allanite-(Nd), and the brighter areas are thorite or throrogummite.

Bastnäsite-(Ce), much like the allanite-(Nd), exhibits depletions in Ce relative to Nd and La (Fig. 6).

## DISCUSSION AND CONCLUSIONS

The Kingman pegmatite is intrusive into Paleoproterozoic orogenic granitic rocks that were emplaced as an outboard collision sutured the Yavapai and Mojave terranes prior to docking with the Laurentian continent (1.71–1.68 Ga) (Duebendorfer *et al.* 2001). The Kingman pegmatite is post-orogenic and was emplaced subsequent to the 1.65 – 1.60 Ga Mazatzal orogeny as a sill-like structure into the newly formed Laurentian crust *ca.* 1.5 Ga. Its emplacement is considered to be contemporaneous with that of the voluminous *ca.* 1.3–1.6 Ga granitic rocks that were emplaced along a belt 600 to 1000 km wide that extends in length from Labrador to the southwestern United States. The parent pluton for this pegmatite is not exposed in the Cerbat Range; it thus either lies at depth and is not exposed, or perhaps it was geographically separated by block faulting during Basin and Range extension. Or perhaps there was no parent pluton (see below).

Although LREE enrichments are common in anorogenic felsic melts, the Kingman pegmatite exhibits an

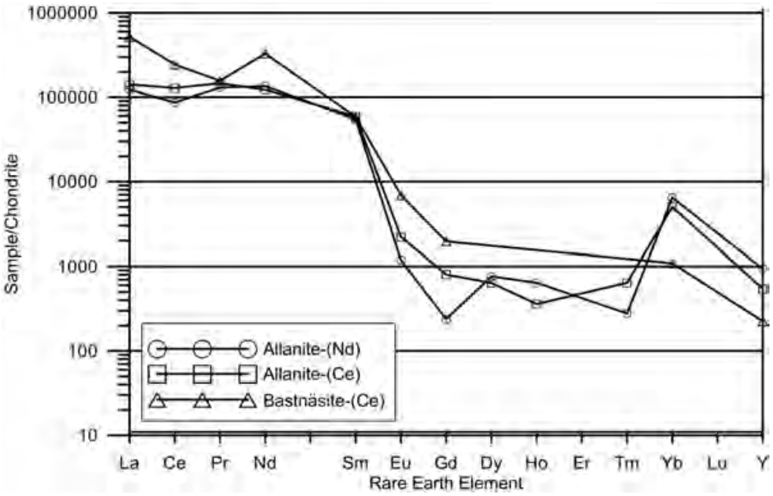

FIG. 6. Chondrite-normalized plot of average compositions of allanite-(Ce), allanite-(Nd) and bastnäsite-(Ce) from the Kingman pegmatite. Normalization factors are from McDonough & Sun (1995).

unusual and extreme level of LREE enrichment, as well as HREE depletion. A LREE enrichment in granitic rocks have been attributed to partial melting of within-plate granite and subsequent partitioning of HREE into a late-stage fluid *via* fluorine complexing (Simmons *et al*. 1987, Gramaccioli *et al*. 1999, Gramaccioli & Pezzotta 2000). The absence of fluorine to act as a HREE complexing agent, as well as the near-absence of HREE-enriched minerals in either the quarry or the dump material, suggest a strong depletion of HREE in the melt that produced the pegmatite. These features are so different from the characteristics of NYF-type pegmatites that occur as segregations in their parent plutons that we conclude that this pegmatite is not likely the result of fractionation derived from a granitic pluton. Recently, several authors have shown that unusual "parentless" pegmatites may be anatectic in origin rather than the result of extreme fractionation of a granitic melt (Martin & De Vito 2005, Ercit 2006). An anatectic origin for the Kingman pegmatite is favored because: 1) it is not associated with a parent granite; 2) it is anomalously depleted in F, Nb, Ta, and HREE, and 3) it is extremely enriched in the LREE, which is consistent with a partial melt derived from continental crust.

The abundance of allanite in the Kingman pegmatite is attributed to an extreme LREE enrichment coupled with a near-absence of P and F, which would have allowed for the formation of either monazite or bastnäsite, respectively. Most of the allanite from the Kingman pegmatite is Nd-rich allanite-(Ce). However some of the samples from the B cut have domains with Nd dominant at the *A*2 site, and thus are allanite-(Nd). These samples represent the fourth world location and the first reported location in the United States for the recently approved allanite-(Nd).

The slight enrichment in Nd and depletion in Ce in allanite-(Nd) relative to the allanite-(Ce) cannot be attributed to alteration by late-stage oxidizing fluids, as oxidation to the less mobile Ce to +4 would preferentially remain, thus leaving the crystals enriched in Ce relative to the other REE (Albio & Nokazi 1999). Thus we suggest that the slight Nd enrichment exhibited in allanite along the rim and along fractures may be related to late-stage alteration of allanite-(Ce) to bastnäsite-(Ce). Carbonate-bearing late-stage fluids may have become more enriched in F, the result of biotite decomposition, producing bastnäsite-(Ce) with slightly lower Nd/Ce values. The redistribution of Ce preferentially to bastnäsite-(Ce) would then lead to greater Nd/Ce values in recrystallized allanite near fractures and along the recrystallized rim.

## ACKNOWLEDGEMENTS

This work was, in part, supported by a faculty research grant from Adrian College and a University of New Orleans student field-research grant. We are grateful to R. Škoda, V. Bermanec, Milan Novák and Robert F. Martin for helpful reviews that greatly improved this manuscript. The authors are pleased to dedicate this paper to Petr Černý in recognition of his many profound contributions to understanding pegmatite mineralogy, petrology, geochemistry, classification, and genesis. The first author is particularly indebted to Petr, as his research and the pegmatite conferences

TABLE 3. AVERAGE COMPOSITIONS OF ALLANITE-(Nd) AND ALLANITE-(Ce) FROM THE KINGMAN FELDSPAR MINE, ARIZONA

| | Allanite-(Nd) | | | Allanite-(Ce) | | | | | |
|---|---|---|---|---|---|---|---|---|---|
| Sample | KFMB-A | KFM-D | KFM-11 | KFMB-A | KFMB-X | KFMC-X | KFMC-F | KFMC-S | KFMC-M |
| *n* | 6 | 5 | 5 | 4 | 8 | 4 | 3 | 5 | 8 |
| $SiO_2$ wt.% | 29.68 | 29.67 | 29.80 | 29.79 | 29.52 | 29.67 | 29.86 | 29.83 | 29.90 |
| $ThO_2$ | 0.82 | 0.85 | 0.55 | 0.50 | 0.39 | 0.71 | 0.98 | 0.93 | 1.19 |
| $UO_2$ | 0.10 | 0.11 | 0.05 | 0.03 | 0.03 | 0.04 | 0.10 | 0.10 | 0.12 |
| $TiO_2$ | 0.56 | 0.52 | 0.56 | 0.78 | 0.68 | 0.37 | 0.94 | 0.91 | 0.93 |
| $Al_2O_3$ | 12.92 | 12.56 | 12.88 | 12.59 | 11.86 | 12.94 | 12.85 | 13.82 | 14.40 |
| $La_2O_3$ | 4.12 | 3.74 | 4.83 | 3.75 | 4.55 | 3.66 | 3.84 | 3.91 | 4.29 |
| $Ce_2O_3$ | 6.60 | 7.04 | 6.34 | 8.88 | 8.69 | 9.12 | 9.97 | 10.05 | 9.34 |
| $Pr_2O_3$ | 1.85 | 1.84 | 1.68 | 1.53 | 1.60 | 1.89 | 0.98 | 1.20 | 1.31 |
| $Nd_2O_3$ | 8.36 | 8.61 | 7.30 | 6.89 | 6.34 | 6.31 | 6.06 | 6.97 | 7.25 |
| $Sm_2O_3$ | 1.13 | 1.16 | 1.14 | 0.99 | 1.14 | 1.14 | 0.80 | 0.59 | 0.55 |
| $Eu_2O_3$ | 0.00 | 0.00 | 0.03 | 0.00 | 0.00 | 0.02 | 0.02 | 0.02 | 0.02 |
| $Gd_2O_3$ | 0.00 | 0.00 | 0.02 | 0.02 | 0.02 | 0.02 | 0.01 | 0.00 | 0.02 |
| $Dy_2O_3$ | 0.03 | 0.03 | 0.02 | 0.03 | 0.00 | 0.02 | 0.00 | 0.03 | 0.04 |
| $Yb_2O_3$ | 0.15 | 0.16 | 0.11 | 0.06 | 0.11 | 0.08 | 0.15 | 0.11 | 0.07 |
| $Y_2O_3$ | 0.18 | 0.18 | 0.13 | 0.09 | 0.09 | 0.09 | 0.23 | 0.15 | 0.11 |
| $Fe_2O_3$ | 7.55 | 7.10 | 7.34 | 7.75 | 8.79 | 7.53 | 8.16 | 7.33 | 6.30 |
| FeO | 10.22 | 10.42 | 10.21 | 10.41 | 9.79 | 9.87 | 9.77 | 10.05 | 10.45 |
| CaO | 9.75 | 9.58 | 9.91 | 9.81 | 10.08 | 9.98 | 9.93 | 10.07 | 10.08 |
| MnO | 1.13 | 1.17 | 1.16 | 1.26 | 0.94 | 1.16 | 1.32 | 1.06 | 1.12 |
| MgO | 0.27 | 0.28 | 0.19 | 0.16 | 0.30 | 0.18 | 0.52 | 0.32 | 0.13 |
| $H_2O$ | 1.46 | 1.44 | 1.45 | 1.48 | 1.45 | 1.46 | 1.49 | 1.50 | 1.50 |
| F | 0.03 | 0.05 | 0.03 | 0.02 | 0.05 | 0.03 | 0.03 | 0.04 | 0.05 |
| Cl | 0.05 | 0.06 | 0.08 | 0.03 | 0.03 | 0.03 | 0.05 | 0.04 | 0.04 |
| -O=F,Cl | -0.03 | -0.04 | -0.03 | -0.02 | -0.03 | -0.02 | -0.02 | -0.02 | -0.03 |
| Total | 96.93 | 96.56 | 95.81 | 96.81 | 96.42 | 96.30 | 98.05 | 99.00 | 99.18 |
| Si *apfu* | 2.979 | 3.002 | 3.005 | 2.988 | 2.984 | 2.991 | 2.955 | 2.928 | 2.929 |
| Al | 0.021 | | | 0.012 | 0.016 | 0.009 | 0.045 | 0.072 | 0.071 |
| Σ*T* site | 3.000 | 3.002 | 3.005 | 3.000 | 3.000 | 3.000 | 3.000 | 3.000 | 3.000 |
| Ti | 0.043 | 0.040 | 0.042 | 0.059 | 0.052 | 0.028 | 0.070 | 0.067 | 0.068 |
| Al | 1.508 | 1.498 | 1.531 | 1.477 | 1.398 | 1.530 | 1.454 | 1.527 | 1.593 |
| $Fe^{2+}$ | 0.858 | 0.881 | 0.861 | 0.874 | 0.828 | 0.832 | 0.809 | 0.825 | 0.857 |
| $Fe^{3+}$ | 0.570 | 0.540 | 0.556 | 0.584 | 0.668 | 0.571 | 0.607 | 0.541 | 0.464 |
| Mg | 0.040 | 0.042 | 0.028 | 0.024 | 0.045 | 0.027 | 0.077 | 0.046 | 0.018 |
| $Mn^{2+}$ | | | | | 0.009 | 0.012 | | | |
| Σ*M* site | 3.018 | 3.002 | 3.020 | 3.017 | 3.000 | 3.000 | 3.017 | 3.007 | 3.000 |
| $Mn^{2+}$ | 0.096 | 0.100 | 0.099 | 0.107 | 0.071 | 0.087 | 0.110 | 0.088 | 0.093 |
| Ca | 1.048 | 1.039 | 1.070 | 1.054 | 1.092 | 1.078 | 1.053 | 1.059 | 1.058 |
| La | 0.025 | 0.023 | 0.030 | 0.023 | 0.028 | 0.022 | 0.024 | 0.024 | 0.026 |
| Ce | 0.040 | 0.043 | 0.039 | 0.054 | 0.053 | 0.056 | 0.061 | 0.061 | 0.057 |
| Pr | 0.011 | 0.011 | 0.010 | 0.009 | 0.010 | 0.011 | 0.006 | 0.007 | 0.008 |
| Nd | 0.050 | 0.051 | 0.043 | 0.041 | 0.038 | 0.037 | 0.036 | 0.041 | 0.043 |
| Sm | 0.006 | 0.007 | 0.007 | 0.006 | 0.007 | 0.007 | 0.005 | 0.003 | 0.003 |
| Eu | 0.000 | 0.000 | 0.000 | 0.000 | 0.000 | 0.000 | 0.000 | 0.000 | 0.000 |
| Gd | 0.000 | 0.000 | 0.000 | 0.000 | 0.000 | 0.000 | 0.000 | 0.000 | 0.000 |
| Dy | 0.000 | 0.000 | 0.000 | 0.000 | 0.000 | 0.000 | 0.000 | 0.000 | 0.000 |
| Yb | 0.001 | 0.001 | 0.001 | 0.000 | 0.001 | 0.000 | 0.001 | 0.001 | 0.000 |
| Y | 0.002 | 0.002 | 0.001 | 0.001 | 0.001 | 0.001 | 0.002 | 0.001 | 0.001 |
| Th | 0.019 | 0.020 | 0.013 | 0.011 | 0.009 | 0.016 | 0.022 | 0.021 | 0.026 |
| U | 0.002 | 0.002 | 0.001 | 0.001 | 0.001 | 0.001 | 0.002 | 0.002 | 0.003 |
| Σ*A* site | 1.982 | 1.997 | 1.975 | 1.983 | 2.000 | 2.000 | 1.983 | 1.993 | 2.000 |
| H | 0.981 | 0.973 | 0.975 | 0.989 | 0.978 | 0.985 | 0.982 | 0.982 | 0.978 |
| F | 0.010 | 0.017 | 0.011 | 0.007 | 0.017 | 0.010 | 0.010 | 0.011 | 0.015 |
| Cl | 0.009 | 0.010 | 0.014 | 0.004 | 0.005 | 0.006 | 0.008 | 0.007 | 0.007 |
| Σ Hydroxyl site | 1.000 | 1.000 | 1.000 | 1.000 | 1.000 | 1.000 | 1.000 | 1.000 | 1.000 |

These compositions were determined using am ARL–SWMQ electron microprobe; n.d.: not detected, *n* number of analyses made. Sought but not detected were: $Tb_2O_3$, $Ho_2O_3$, $Er_2O_3$, $Tm_2O_3$, $Lu_2O_3$, $Na_2O$, PbO. Total iron was partitioned into $Fe^{2+}$ and $Fe^{3+}$ to yield a total of 25 charges. The amount of $H_2O$ was calculated to yield a total of 1 OH + F + Cl.

he organized, filled with stimulating conversations, inspired her as a graduate student to continue pegmatite research. For this reason, she is honored to be a contributor to this thematic issue of *The Canadian Mineralogist* designed as a tribute to Petr Černý.

## REFERENCES

ALBIO, D.S. & NOKAZI, Y. (1999): Rare earth elements in seawater: particle association, shale-normalization and Ce oxidation. *Geochim. Cosmochim. Acta* **63**, 363-372.

APPLEMAN, D.E. & EVANS, H.T., JR. (1973): Job 9214: indexing and least-squares refinement of powder diffraction data. *U.S. Geol. Surv., Comput. Contrib.* **20** (*NTIS Doc.* **PB2–16188**).

ARMBRUSTER,T., BONAZZI, P., AKASAKA, M., BERMANEC, V, CHOPIN, C., GIERÉ, R., HEUSS-ASSBICHLER, S., LIEBSCHER, A, MENCHETTI, S., PAN, YUANMING & PASERO, M. (2006): Recommended nomenclature of epidote-group minerals. *Eur. J. Mineral.* **18**, 551-567.

ČERNÝ, P. & ERCIT, T.S. (2005): The classification of granitic pegmatites revisited. *Can. Mineral.* **43**, 2005-2026.

CONDIE, K.C. (1986): Geochemistry and tectonic setting of Early Proterozoic supracrustal rocks in the southwestern United States. *J. Geol.* **94**, 845-864.

DUEBENDORFER, E.M., CHAMBERLAIN, K.R. & JONES, C.S. (2001): Paleoproterozoic tectonic history of the Cerbat Mountains, northwestern Arizona: implications for crustal assembly in the southwestern United States. *Geol. Soc. Am., Bull.* **113**, 575-590.

ERCIT, T.S. (2002): The mess that is "allanite". *Can. Mineral.* **40**, 1411-1419.

ERCIT, T.S. (2006): Ta–Nb geochemical constraints on the petrogenesis of granitic pegmatites in the southwestern Grenville Province, Ontario. *Geol. Asoc. Can. – Mineral. Assoc. Can., Abstr. Program* **31**, 46.

GONZÁLEZ DEL TÁNAGO, J. (1997): Allanita-(Nd) y minerals de elementos raros en las pegmatites graníticas de La Cabrera, Madrid. *Rev. Soc. Geol. España* **10**, 83-105.

GRAMACCIOLI, C.M., DIELLA, V. & DEMARTIN, F. (1999): The role of fluoride complexes in REE geochemistry and the importance of 4f electrons: some examples in minerals. *Eur. J. Mineral.* **11**, 983-992.

GRAMACCIOLI, C.M. & PEZZOTTA, F. (2000): Geochemistry of yttrium with respect to the rare-earth elements in pegmatites. *Memorie della Italiana di Scienze e del Museo Civico di Storia Naturale di Milano* **XXX**, 111-115.

HANSON, S.L., FALSTER, A.U. & SIMMONS, W.B. (2007): Rare-earth mineralogy of the Mohave County pegmatites, northwestern Arizona. *Rocks & Minerals* **82**, 236-237.

HEINRICH, E.W. (1960): Some rare-earth mineral deposits in Mojave County, Arizona. *Arizona Bureau of Mines, Bull.* **167**.

KAY, R.W. & MAHLBURG-KAY, S. (1993): Delamination and delamination magmatism. *Tectonophysics* **219**, 177-189.

MARTIN, R.F. & DE VITO, C. (2005): The patterns of enrichment in felsic pegmatites ultimately depend on tectonic setting. *Can. Mineral.* **43**, 2027-2048.

MCDONOUGH, W.F. & SUN, S.-S. (1995): The composition of the Earth. *Chem. Geol.* **120**, 223-253.

MCLELLAND, J., DALY, S.J. & MCLELLAND, J.M. (1996): The Grenville orogenic cycle (*ca.* 1350–1000 Ma): an Adirondack perspective. *Tectonophysics* **265**, 1-28.

MCLELLAND, J.M., SELLECK, B.W., HAMILTON, M.A. & BICKFORD, M.E. (2010): Late- to post-tectonic setting of some major Proterozoic anorthosite – mangerite – charnockite – granite (AMCG) suites. *Can. Mineral.* **48**, 729-750.

MINAKAWA, T., FUNAKOSHI, N. & MORIOKA, H. (2001): Chemical properties of allanite from the Ryoke and Hirosima granite pegmatites in Shikoku, Japan. *Mem., Faculty of Science, Ehime Univ.* **7**, 1-13.

POUCHOU, J.-L. & PICHOIR, F. (1991): Quantitative analysis of homogeneous or stratified microvolumes applying the model "PAP". *In* Electron Probe Quantitation (K.F.J. Heinrich & D.E. Newbury, eds.). Plenum Press, New York, N.Y. (31-75).

SIMMONS, W.B., HANSON, S.L. & FALSTER, A.U. (2006): Samarskite-(Yb): a new species of the samarskite group from the Little Patsy pegmatite, Jefferson County, Colorado. *Can. Mineral.* **44**, 1119-1125.

SIMMONS, W.B., LEE, M.T. & BREWSTER, R.H. (1987): Geochemistry and evolution of the South Platte granite–pegmatite system, Jefferson County, Colorado. *Geochim. Cosmochim. Acta* **51**, 455-471.

SIMMONS, W., WEBBER, K., FALSTER, A.U., HANSON, S. & BROWN, T.J. (2011): Geochemistry of REE-rich pegmatites from different tectonomagmatic provinces in South Platte, CO, Trout Creek Pass, CO, Kingman and Aquarius Range, AZ, North America. *Contrib. 5th Int. Symp. on Granite Pegmatites* (*Mendoza*), *Program Abstr.*, 13-16.

ŠKODA, R., CEMPÍREK, J., FILIP, J. & NOVÁK, M. (2010): Allanite-(Nd), IMA 2010–060. CNMNC Newsletter No. 8. *Mineral. Mag.* **75**, 289-294.

SUGITANI, Y., SUZUKI, Y. & NAGASHIMA, K. (1984): Recovery of the original samarskite structure by heating in a reducing atmosphere. *Am. Mineral.* **69**, 377-379.

SUGITANI, Y., SUZUKI, Y. & NAGASHIMA, K. (1985): Polymorphism of samarskite and its relationship to other structurally related Nb–Ta oxides with the α-$PbO_2$ structure. *Am. Mineral.* **70**, 856-866.

WASSERBURG, G.J. & LANPHERE, M.A. (1965): Age determinations in the Precambrian of Arizona and Nevada. *Geol. Soc. Am., Bull.* **76**, 735-758.

WHITMEYER, S.J. & KARLSTROM, K.E. (2007): Tectonic model for the Proterozoic growth of North America. *Geosphere* **3**, 220-259.

WINDLEY, B.F. (1993): Proterozoic anorogenic magmatism and its orogenic connections. *J. Geol. Soc. London* **150**, 39-50.

WOODEN, J.L. & MILLER, D.M. (1990): Chronologic and isotopic framework for Early Proterozoic crustal evolution in the eastern Mojave Desert region, SE California. *J. Geophys. Res.* **95**, 20,133-20,146.

WOODEN, J.L., STACEY, J.S., DOE, B., HOWARD, K.A. & MILLER, D.M. (1988): Pb isotopic evidence for the formation of Proterozoic crust in the southwestern United States. *In* Metamorphism and Crustal Evolution of the Western United States: Rubey Volume VII (W.G. Ernst, ed.). Prentice Hall, Englewood Cliffs, New Jersey (68-86).

*Received June 23, 2011, revised manuscript accepted July 8, 2012.*